# Effects of the magnetic field model and wave polarisation on the estimation of proton number densities in the magnetosphere using field line resonances

*C.L. Waters[a], K. Kabin[b], R. Rankin[b], E. Donovan[c] J. C. Samson[b]*

*[a]School of Mathematical and Physical Sciences, University of Newcastle, Callaghan, 2308, New South Wales, Australia*
*[b]Physics Department, University of Alberta, Edmonton, Alberta, Canada, T6G2J1*
*[c]Department of Physics and Astronomy, University of Calgary, Calgary, Alberta, Canada, T2N1N4*

**Abstract**
The cold, core plasma mass density in the Earth's magnetosphere may be deduced from the resonant behaviour of ultra-low frequency (ULF; 1-100 mHz), magnetohydrodynamic (MHD) waves. Ground based magnetometers are the most widely used instruments for recording the signature of ULF wave activity in the magnetosphere. For a suitable model of the background magnetic field and a functional form for the variation of the proton number density with radial distance, the resonant frequencies of ULF waves provide estimates of the equatorial plasma mass density. At high latitudes, the magnetic field model becomes critical when estimating the plasma mass density from FLR data. We show that a dipole field model is generally inadequate for latitudes greater than ~65$^{o}$ geomagnetic compared with models that are keyed to magnetic activity, interplanetary magnetic field and solar wind properties. Furthermore, the method often relies on the detection of the fundamental ULF resonance, which changes frequency depending on the polarisation of the oscillation. Using idealised toroidal and poloidal oscillation modes, the range of the derived densities as the ULF wave polarisation changes is of the same order as changing the density function from a constant value throughout the magnetosphere to assuming constant Alfven speed in a dipole geometry.

*Keywords:* ULF waves, remote sensing, magnetosphere plasma mass density, field line resonances

## 1. Introduction

It is generally accepted that small amplitude (1-10 nT), ultra low frequency (ULF; 1-100 mHz) variations of the geomagnetic field are the manifestation of magnetohydrodynamic (MHD) wave activity in the magnetosphere which may be observed on the ground at almost any latitude and local time. The energy source for these waves is attributed to a number of processes that arise from the interaction of solar wind plasma with the Earth's magnetic field in space. The Kelvin Helmholtz instability [*Southwood*, 1968], impulses at the magnetopause from solar wind pressure variations [*Sibeck*, 1994] and upstream ion cyclotron waves are thought to be the main ULF wave generation mechanisms. Knowledge of the energy source(s) for ULF waves in the magnetosphere may provide insight into the local time and magnetic activity dependency, propagation and generation properties of ULF waves, details which are still debated. However, a complete knowledge is not necessary when using these oscillations to estimate plasma mass density in the magnetosphere.

Within the magnetosphere, cold plasma MHD theory predicts two ULF wave modes: the compressional or fast mode and a shear Alfven wave or 'transverse' mode. The theory describing MHD wave oscillations in the magnetosphere is well known [*Dungey*, 1954; *Sen*, 1965; *Tamao*, 1966; *Radoski*, 1970; *Chen and Hasegawa*, 1974; *Southwood*, 1974]. A key

characteristic of the shear Alfven mode is the propagation of wave energy along the geomagnetic field. Suitable conditions for wave reflection in the ionospheres located at each 'end' of a magnetic 'field line' allows field line resonances (FLRs). The FLR frequency depends on the distance along the background magnetic field between the reflection points in the conjugate ionospheres, the magnetic field magnitude and the plasma mass density distributed along the resonant region.

The spatial structure of FLRs, measured at the ground, has been described by a number of researchers [*Krylov and Federov,* 1976; *Hughes and Southwood*, 1976; *Kivelson and Southwood*, 1986]. Essentially a shear Alfven wave at the appropriate resonant magnetic shell becomes localised in latitude. The localisation depends on the duration and amplitude of the source energy balanced against losses which are largest in the ionospheres. For a well developed resonance, the latitude profile exhibits a characteristic amplitude and phase change across the resonant region, facilitating detection in magnetometer records. The possibility of using FLRs to diagnose the structure of the magnetosphere was soon recognised (eg. *Obayashi and Jacobs*, 1958; *Troitskaya and Gul'elmi,* 1967) and techniques using realistic magnetic field models, capable of routinely determining magnetospheric proton number densities out to $12R_E$ in near real time have been developed [*Waters et al*., 1996].

The essential elements for remote sensing the plasma mass density in the magnetosphere, given FLR data, were described by *Cummings et al.* (1969) who used data from the ATS 1 satellite. Assuming a hydrogen plasma, the functional form for the density, $\rho$, that depends on the radial distance, r, from the centre of the Earth was

$$\rho=\rho_0(r_0/r)^{\gamma} \tag{1}$$

Given a value for the FLR frequency, the task is to solve for $\rho_0$ at $r_0$. The parameter $\gamma$ is usually set equal to 3 or 4. The linearised equations for shear Alfven waves in a stationary, cold plasma are

$$\mu_0 \rho \frac{\partial \mathbf{v}}{\partial t} = (\nabla \times \mathbf{B}) \times \mathbf{b} + (\nabla \times \mathbf{b}) \times \mathbf{B} \tag{2}$$

$$\frac{\partial \mathbf{b}}{\partial t} = \nabla \times (\mathbf{v} \times \mathbf{B}) \tag{3}$$

where **B** is the background magnetic field, **b** is the wave perturbed magnetic field and **v** is the perturbation plasma velocity due to the wave. *Cummings et al*. (1969) and others (eg. *Orr*, 1973) have assumed a dipole magnetic field geometry. In general, a nonuniform magnetic field couples the fast and shear Alfven wave modes. For a dipole field model, *Orr* (1973) summarised three cases that decouple the wave equations. Assume the perturbation has a longitudinal variation given by $e^{im\varphi}$ where $\varphi$ is the longitude and *m*, the azimuthal wave number (*Olson and Rostoker*, 1978). For *m*=0, the axially symmetric toroidal equation describes a shear Alfven oscillation of a magnetic shell with field aligned Poynting flux. The poloidal case for *m*=0 is the fast mode that symmetrically expands and compresses the magnetosphere, with Poynting flux across field lines. The third case is for large *m*, the guided poloidal mode of *Radoski* (1967), where the Poynting flux is field aligned again.

*Singer et al*. (1981) derived the linearised wave equation for a cold, collisionless, magnetised plasma in a form suitable for a general background magnetic field geometry. The key to their method is the $h_\alpha$ geometric factors. Consider two field lines separated by a distance $h_\alpha$ in the plane normal to the field direction. At any location along one of the field lines, define $h_\alpha$ by requiring that the separation be equal to $h_\alpha\delta_\alpha$. If the normal unit vector between the field lines

is **α** then for a small plasma displacement, $\xi_\alpha$ in the **α** direction, the wave equation is

$$\frac{\partial^2}{\partial s^2}\left(\frac{\xi_\alpha}{h_\alpha}\right)+\frac{\partial}{\partial s}\left(\frac{\xi_\alpha}{h_\alpha}\right)\frac{\partial}{\partial s}\ln\left(h_\alpha^2 B\right)+\frac{\mu_0\rho\omega^2}{B^2}\left(\frac{\xi_\alpha}{h_\alpha}\right)=0 \qquad (4)$$

where B is the background magnetic field magnitude, *s* is a distance along the field line, and ω is the frequency. For the results presented here, Eq. (4) was numerically solved using a fourth order Runge-Kutta algorithm. Since both ρ and ω appear in the same term, they have been combined into a single variable in our solver routines, allowing for either a solution for ω, given ρ or a solution for the mass density, ρ, given ω. The plasma mass density, ρ, depends on *s*. In particular, the last term of Eq. (4) involves the Alfven speed,

$$V_A(s)=\frac{B(s)}{\sqrt{\mu_0\,\rho(s)}} \qquad (5)$$

where the dependence on the field line coordinate, *s* is emphasised. Since the last term in Eq. (4) involves the inverse of $V_A$, the weighting from $V_A$ in the solution is larger for regions where the Alfven speed is small, i.e. near the equatorial plane. Therefore, for latitudes where the magnetic field maps into the plasmatrough region of the magnetosphere, Eq. (1) need only be a reasonable approximation to the variation of the plasma mass density out near the equatorial plane. The sharp increase in the Alfven speed near the ionosphere does not greatly affect the solution. This is not the case for low latitudes (L<~2) where alternative methods for estimating the plasma mass density are desirable (*Price et al.*, 1999). However, in low latitude regions, the procedure is simplified as a dipole background magnetic field is usually suitable.

As pointed out by *Singer et al.* (1981), Eq. (4) is a one dimensional equation and applies to strictly transverse perturbations (**B•b**=0); i.e. the wave bends but does not compress the magnetic field. The only information used in the solution involves two nearby field lines. If **α**, the field line separation vector, points in the azimuthal direction then we solve for the uncoupled toroidal wave mode. The symmetric poloidal mode is simulated for two field lines located in a meridian plane. Furthermore, Eq. (4) was obtained from the linearised system of MHD equations and neglects the first term on the right hand side of Eq. (2) which describe effects arising from background currents (**J×b** force). Singer et al argue that this term is insignificant for the field model used. Some of the consequences of these restrictions and the extension to solutions that are sensitive to the magnetic field geometry and allow wave mode coupling are discussed later and in the companion paper in this issue (*Kabin et al.*, 2006).

## 2. FLRs and Mass Density in the Plasmatrough

Estimating plasma mass densities in the plasmatrough region of the magnetosphere using ground based magnetometer signatures of ULF field lines resonances was described by *Waters et al.* (1995, 1996). The magnetometer data from the 'Churchill line' magnetometer sites in the CANOPUS array (*Samson et al.*, 1992) are used. Coordinates for the midpoint locations of these magnetometers are listed in Table 1. In this section, the observed FLRs are used to estimate the plasma mass density in the equatorial plane. The results using different background magnetic field models and the toroidal and poloidal ULF wave modes are compared.

### *2.1 Toroidal mode: Effect of Magnetic Field Models for Low Magnetic Activity*

The latitudinal and temporal variation of FLRs is identified using cross spectral phase spectra calculated using the north-south sensor components of pairs of latitudinally located

magnetometers (*Waters et al*., 1991). An example is shown in Fig. 1. The cross phase is maximum at the resonant frequency for the latitude that is midway between the two magnetometers. The data were recorded during 9 February, 1995 by the seven fluxgate magnetometers in the 'Churchill line' from the CANOPUS fluxgate magnetometer array (Table 1). This interval represents a magnetically quiet period with Kp~0 for the whole day. Due to the FLR dependence on field line length, the resonant frequencies increase as the latitude decreases. For data that show harmonics, as seen for example in the RAN:ESK data, the fundamental is chosen. The implications of estimating plasma mass densities from the fundamental involve the wave polarisation and are discussed later. The temporal variation of the FLRs depends on changes in both the plasma mass density and the magnetic field as the magnetometers rotate with the Earth. In order to extract estimates of the plasma mass density, a suitable background magnetic field model is required.

The plasma mass densities in the equatorial plane can be estimated using Eq. (4). The $\omega$ are the FLRs, obtained from the maximum phase difference traces through the cross phase spectra in Fig. 1. The background magnetic field was constructed from the addition of the T01_01 (*Tsyganenko*, 2002) magnetosphere model with the IGRF95 main field model. The plasma mass density (kg $m^{-3}$) is converted to equivalent proton number density (per cm) and the resultant values for the Geocentric Solar Magnetospheric (GSM) equatorial plane are shown in Fig. 2. Other techniques are required in order to determine the ion mixture [e.g. *Dent et al.,* 2003; *Menk et al.,* 2004].

The dependence of the proton number densities obtained from the FLR data in Fig. 1 and Eq. (4) using different background magnetic field models is shown in Fig. 3. The dipole magnetic field model (solid) gives larger number densities at high latitudes. This is due to the absence of field line stretching in this model. By ~$65^0$, all the magnetic field models yield similar density values, providing a guide to the latitude range where the simple dipole approximation is reasonable for these quiet magnetic conditions. The two highest latitude magnetometer pairs of RAN:ESK and ESK:FCH highlight the differences in densities due to the magnetic field models. The differences are greater during the afternoon with the T01_01 model consistently giving smaller densities and the T89 (*Tsyganenko*, 1989) model, the larger values out of the three Tsyganenko field models.

Fig. 4 shows the magnetic field parameters in the GSM equatorial plane, i.e. where $Z_{GSM}$=0. Fig 4(a) reveals the shift in MLT at the location where the mapped field lines cross the $Z_{GSM}$=0 plane, compared with the MLT at 120 km altitude in the northern hemisphere. As pointed out by *Singer et al*. (1981), for remote sensing mass densities using ground based measurements of FLRs, the MLT at the ground does not necessarily correspond with a similar MLT in space near the equatorial plane, the region where the FLR is most sensitive to the density. One may need to swing the MLT around by up to 4 hours, even for quiet magnetic conditions. Therefore, the x-axis in Fig. 3 is the MLT out in the magnetosphere where $Z_{GSM}$=0. Fig. 4(b) shows the radial distance, measured from the Earth centre, to the $Z_{GSM}$=0 crossing point for each field line mapping. The three Tsyganenko magnetic field models consistently show why the dipole model is unsuitable for mapping from these latitudes. We can also see why the T01_01 model gives smaller proton number densities in Fig. 3. As shown in Fig. 4(b) the T01_01 model consistently maps to larger radial distances. For a given FLR frequency, the longer T01_01 field 'lines' yield smaller density values.

*2.2 Toroidal mode: Effect of Geomagnetic Field Models for Active Periods*

The level of magnetic activity influences the magnetic field in space. In order to investigate

the effects of increased magnetic activity on estimates of proton number density for the different field models, the values for the FLRs obtained for 9 February, 1995 were used while the input parameters for the magnetic field models were changed to those from a more active day. Initially, the active day was chosen as 7 April, 1995 where Kp reached 8. The input parameters to the T96_01 (*Tsyganenko and Stern*, 1996) and T01_01 magnetic field models calculated for this period from WIND satellite measurements exceeded the recommended range for the IMF values and solar wind pressures for these field models. This illustrates a limitation imposed by magnetic field models when estimating proton number densities in the magnetosphere. Even if FLRs can be obtained from ground magnetometer data for very active periods, the proton number density should not be computed for magnetic field parameters that exceed the recommended range.

Scanning the Kp magnetic index history and starting at 9 February, 1995, the geomagnetic activity increased to moderate Kp levels on the 11 February. By the 13 February, Kp was hovering between 5 and 6, so this day was chosen to represent a more magnetically active period. The solar wind parameters obtained from the WIND spacecraft for 13 February, 1995 were used in the T96_01 and T01_01 magnetic field models, taking into account the delay time based on the solar wind speed. Kp was set to 6 for the T89 model and the FLR values for each magnetometer pair found from Fig. 1 were used. The resultant proton number densities are shown in Fig. 5. The late afternoon increase in proton number density seen at higher latitudes in Fig. 3 has disappeared for calculations that used the Tsyganenko field models, down to the BAC:GIL pair. The dipole field model consistently overestimates the densities compared with the Tsyganenko models, a feature of the field line stretching that occurs. All three Tsyganenko models give similar trends in the density with time. Even at the lower latitude for GIL:ISL there is evidence for magnetic field distortion as late as 20 MLT. The arch shape, MLT variation of the FLR frequency is clearly seen at RAN:ESK and ESK:FCH, a feature of FLRs seen at high latitudes previously discussed by *McHarg et al.* (1994) and *Waters et al.*, (1995). It is not surprising to see the arch appear here in the number density since Eq. (4) shows that one may provide $\rho$ and solve for $\omega$ or the reverse.

The differences in the magnetic field models for active magnetic conditions becomes apparent when comparing the MLT at the GSM equatorial plane compared with the time near the ground. Fig. 6(a) shows the rather unique behaviour when using the T89 model in this regard. The vertical axis is the MLT value derived from the location where $Z_{GSM}=0$, in space subtracted from the MLT at the ground (gnd_MLT). We see negative MLT shifts in the morning, switching over to positive shifts for the afternoon for the RAN:ESK latitude. At lower latitudes, indeed by the next magnetometer pair (ESK:FCH), all four magnetic field models give a similar trend of the MLT shift with time. Positive values indicate that the MLT value in the equatorial plane is larger (later in time) compared with the MLT at the ground.

The MLT shifts with time are consistent with field lines swept back from the dayside (see also Fig 4 in *Singer et al.*, 1981). Fig. 6(b) shows the northern hemisphere trace of field lines projected onto the XY (GSM) plane. Dawn is toward the bottom and noon to the right of the figure. Each magnetic field line begins at 120 km altitude and ends where $Z_{GSM}=0$. The location where $Z_{GSM}=0$ is not necessarily where the maximum distance from Earth occurs. Comparisons of the magnetic field models shown in Fig. 6 represent geometries close to the open/closed field line boundary as indicated by the large number of mappings that are absent from the nightside in Fig. 6(b). These were classified by the computer algorithm as 'open' field lines and deleted from the computations. For estimating the plasma number density,

field line traces were computed for each 15 minute interval in MLT, keeping the start latitude and longitude constant. One example where a 15 minute change makes quite a difference to the field mapping results is seen in the T89 case for the mapped field lines near dusk. One 'rogue' field line is swept further tailward compared with the adjacent field lines. Therefore, for active periods, one needs to be aware that the various magnetic field model geometries can differ greatly in regions that map from higher latitude locations of magnetometer arrays, yielding an associated uncertainty in number density estimates. Fortunately, consistent results are obtained from the models by moving a few degrees equatorward.

*2.3 Toroidal compared with Poloidal Mode*

The calculation of proton number densities from FLR data is usually computed from the toroidal mode solution to the wave equation, using the fundamental resonance. However, the twisting and distortion of the background magnetic field in addition to the properties of the mechanism for generating the resonance in the first place means that the assumption of a purely uncoupled toroidal mode oscillation (the $\alpha$ in the azimuthal direction) is probably not valid along most of the field line. The first step to investigating this affect is to calculate the range of values for the proton number density when specifying purely toroidal compared with purely poloidal oscillations in the computations. While this does not fully address the approximation of zero coupling to nearby field lines (solving the self-consistent problem), the exercise should provide a useful uncertainty range for the estimated densities, recognising that the transverse perturbation may not be purely azimuthal or radial.

*Cummings et al.* (1969) showed that when using a dipole magnetic field, the fundamental toroidal mode FLR is ~30% higher in frequency compared with the poloidal mode. Higher harmonics showed essentially the same frequencies for the toroidal and poloidal (uncoupled) modes. Using the FLR values from Fig. 1, the number densities were computed from the IGRF95+T01_01 magnetic field model, using the parameters from both the quiet (9 Feb. 1995) and the active period (13 Feb 1995) and assuming an uncoupled toroidal fundamental oscillation. Using the same set of resonant frequencies, the number densities were then calculated for fundamental poloidal oscillations.

Fig. 7 shows the resulting percentage difference in the densities for the uncoupled toroidal and poloidal modes, using the IGRF+T01 field model and assuming the same FLRs. Fig. 7(a) shows that even for quiet magnetic conditions, the mass densities obtained when using the fundamental uncoupled toroidal resonant frequencies exceed those when assuming poloidal oscillations by up to 75% on the nightside while toward noon at the higher latitudes, the densities obtained using poloidal oscillations are larger. This effect is enhanced for the active period as shown in Fig. 7(b).

## 3. Discussion

In this paper we have discussed the equatorial plasma density values in the Earth's magnetosphere obtained by using ground based magnetometer measurements and different magnetic field models. The procedure assumes some special conditions for the plasma perturbations and the background magnetic field. Most recent estimates of plasma mass density in the magnetosphere (e.g. *Dent et al*., 2003; *Berube and Moldwin*, 2003; *Menk et al*., 2004) using ULF wave resonances detected on the ground have essentially followed the procedure outlined by *Cummings et al.* (1969). This assumes purely transverse oscillations with the azimuthal wave number set to zero to describe the toroidal, shear Alfven mode, which does not couple wave energy to nearby field lines. While there has been some

preliminary research on solving the self-consistent, coupled wave problem in both two and three dimensional geometries (eg. *Wright*, 1992; *Klimushkin et al*., 1995; *Rankin et al*. 2004), it is not clear how the plasma mass density estimates might be affected by mode coupling. When the range of plasma mass density estimates are found for the mixed mode solutions, Fig. 7 provides a comparison to ascertain whether the computationally more simple approach is adequate. In the meantime, while the much more complicated self-consistent solutions are sought, the comparison between plasma mass density estimates using purely toroidal and purely poloidal eigenfrequencies (Fig. 7) are expected to provide reasonable limits on the range of expected densities for mixed mode solutions.

The second assumption involves an inconsistency between Eq. (4) and the magnetic field models used. The Tsyganenko field models show distortion from a dipole configuration arising from background electric currents, $\nabla \times \mathbf{H} = \mathbf{J}$. While *Singer et al*. (1981) argued that this effect on the wave equation is small for the Olson-Pfitzer field model, $\mathbf{J} \times \mathbf{b}$ force effects would depend on the activity level prescribed for the Tsyganenko models, becoming more important at high latitudes. A further inconsistency in the procedure concerns the existence of uncoupled ULF wave modes in distorted field geometries. *Wright and Evans* (1991) have discussed the magnetic field topologies that can support uncoupled, cold plasma wave modes. Even in a dipole geometry, while purely toroidal oscillations decouple, the purely poloidal oscillations do not. Therefore, Wright and Evans state that "azimuthal field perturbations will be longer lived than their poloidal counterparts". In addition to the magnetic field, Table 1 in *Wright and Evans* (1991) restricts the models that can support uncoupled modes according to the spatial variation of the plasma mass density so uncoupled cold plasma wave modes appear unlikely to be the case in practice.

Using different magnetic field models yields different estimates for the plasma mass density. The Tsyganenko models attempt to accurately model field line stretching and distortions from a dipole geometry. These are complex models based on multiple satellite data sources and parameterisation of various current systems in the magnetosphere. Improvements and discussions regarding the accuracy of the magnetic field values may be found in the literature that describes each new version of the Tsyganenko model and is not within the scope of this paper. However, we are concerned about whether the plasma mass density estimates obtained using the various models are close to reality. Therefore, comparisons of the remote sensed mass density estimates with *in-situ* measurements are crucial. The agreement with *in-situ* data using the idealised approach (e.g. *Loto'aniu et al*., 1999; *Dent et al.*, 2003) suggests that effects from the different Tsyganenko field models, coupled wave modes and background currents may not be all that important for estimating the mass density. However, these studies presented comparisons between *in-situ* and remote sensed mass densities near and in regions earthward of geosynchronous orbit. More comparisons at higher latitudes are required. The expected range of plasma mass densities when using different field models at these higher latitudes has been quantified here.

Finally, we compared the variation in the plasma mass density when using different field models and wave polarisation with the variation obtained for different $\gamma$ in Eq. (1). The densities using the T01_01 model and for the 9 February, 1995 data are shown in Fig. 8. In general, the density values are slightly smaller for $\gamma$=6 (dotted line) compared with $\gamma$=0 (solid line) and therefore weakly depend on the value of $\gamma$. For $\gamma$=0, we have no variation of density with radial distance while $\gamma$=6 gives constant Alfven speed along the equator in a dipole magnetic field with slight variation in latitude. Comparison with Fig. 3 shows that variations in densities obtained using the three Tsyganenko field models are smaller than those bounded

by the solid and dotted lines in Fig. 8. Using a dipole field gives significantly larger variations. Figure 8 also shows the densities that would be obtained if the oscillation was assumed to be poloidal (dashed line). The variation in density values obtained for the two polarisations (toroidal and poloidal), are of the same order as those with constant density throughout the magnetosphere ($\gamma$=0) compared with $\gamma$=6.

## 4. Conclusions

The equatorial plasma mass density in the Earth's magnetosphere may be estimated using ground based magnetometer measurements. We compared and contrasted results from a typical magnetically quiet and a day with significant geomagnetic activity. For both events, the cross-phase technique was used to infer the FLR frequencies from the CANOPUS magnetometer measurements. This technique allows us to compute the frequencies at the mid points between the magnetometer stations. While reconstruction of the magnetospheric mass densities is possible in both the quiet and disturbed case, a geomagnetically active day represents a more challenging case, primarily because of the uncertainties associated with the magnetic field models under these conditions. Once the solar wind, IMF or Dst parameters exceed the recommended range for data-constrained Tsyganenko models, the density estimations certainly become unreliable.

We have used the IGRF95 plus T89, T96_01, T01_01 as well as dipole magnetic field models. Our results show that the dipole approximation generally requires unrealistically large mass densities to explain the observed resonant frequencies. This effect is naturally the largest at high CGM latitudes, but even for the CANOPUS magnetometer pair closest to the equator (Island Lake – Pinawa) there is a considerable over-estimation of the mass densities if a dipole magnetic field is used. In contrast, the differences arising from using T89, T96_01 or T01_01 magnetic field models are relatively minor throughout most of the dayside magnetosphere, especially for quiet magnetospheric conditions. Larger differences between the models occur for latitudes that map near the magnetopause. We also find that all Tsyganenko field models adequately explain the observed diurnal variation in the resonant frequencies, while the dipole model does not.

In the present work we have used the wave equation from *Singer et al.*, (1981) to describe the transverse shear Alfven wave along the field line. This equation assumes idealised oscillations and uncertainties related to using different FLR models are discussed in a companion paper (*Kabin et al.*, 2006). Density estimates also depend significantly on the assumption of either a toroidal or poloidal oscillation mode used in the inversion process. These differences vary with MLT and distance from the Earth and in places may be as large as 70%. We have also discussed the variation of the MLT along the magnetic field lines which is different for the different field models and has to be accounted for in reconstructing the plasma mass density in the equatorial plane. In general, we feel that the inversion techniques used to compute the magnetospheric mass densities from the ground-based magnetometer data are approaching sufficient maturity, allowing them to be used routinely in near real time to monitor the plasma content of the magnetosphere. With the expansion of existing magnetometer chains around the world we expect to be able to achieve nearly continuous two-dimensional data coverage in the future.

## References


Berube, D., Moldwin, M.B., Weygand, J., 2003. An automated method for the detection of field line resonance frequencies using ground magnetometer techniques, *J. Geophys. Res.*, *108*(A9), 1348, doi:10.1029/2002JA009737.

Chen, L., Hasegawa, A., 1974. A theory of long-period magnetic pulsations 2. Impulse excitation of surface eigenmode, J. Geophys. Res., 79, 1033.

Cummings, W.D., O'Sullivan, R.J., Coleman, P.J., 1969. Standing Alfvén Waves in the Magnetosphere, J. Geophys. Res., 74, 778.

Dent, Z.C., Mann, I.R., Menk, F.W., Goldstein, J., Wilford, C.R., Clilverd, M.A., Ozeke, L.G., 2003. A coordinated ground-based and IMAGE satellite study of quite-time plasmaspheric density profiles, Geophys. Res. Lett., 30, 2-1 - 2-4.

Dungey, J.W., 1954. Electrodynamics of the outer atmosphere, Penn. State Uni., Ionos. Res. Lab. Sci. Rep. No. 69.

Hughes W.J., Southwood D.J., 1976. The Screening of Micropulsation Signals by the Atmosphere and Ionosphere, J. Geophys. Res., 81, 3234.

Kabin, K., Rankin R., Waters C.L., Marchand R., Donovan E. F., Samson, J.C., 2006. Different models for field line resonances in cold plasma: Effect on magnetospheric density estimation, Planet. Space Sci., this issue.

Kivelson, M.G., Southwood D.J., 1986. Coupling of global magnetospheric MHD eigenmodes to field line resonances, J. Geophys. Res., 91, 4345.

Klimushkin, D.Y., Leonovich, A.S., Mazur, V.A., 1995. On the propagation of transversally-small-scale standing Alfven waves in a three-dimensionally inhomogeneous magnetosphere, J. Geophys. Res., 100, 9527.

Krylov A.L., Federov E.N., 1976. Natural oscillations of a confined volume of magnetized plasma, Dokl. Akad. Nauk SSSR, 231, 68.

Loto'aniu, T.M., Waters, C.L., Fraser, B.J., 1999. Plasma mass density in the plasmatrough: Comparison using ULF waves and CRRES, Geophys. Res. Lett., 26, 3277.

McHarg, M.G., Olson J.V., Newell P.T., 1994. ULF cusp pulsations; Diurnal variations and interplanetary magnetic field correlations with ground based observations, J. Geophys. Res., 100, 19729.

Menk, F.W., Mann, I.R., Smith, A.J., Waters, C.L., Clilverd, M.A., Milling, D.K., 2004. Monitoring the plasmapause using geomagnetic field line resonances, J. Geophys. Res., 109, A04216, doi:10.1029/2003ja010097.

Obayashi, T., Jacobs J.A., 1958.Geomagnetic pulsations and the earth's outer atmosphere, Geophys. J. R. astron. soc., 1, 53.

Olson, J.V., Rostoker, G., 1978. Longitudinal phase variations of Pc4-5 Micropulsations, J. Geophys. Res., 83, 2481.

Orr, D., 1973. Magnetic pulsations within the magnetosphere: A review, J. Atmos. Terr. Phys., 35, 1.

Price, I.A., Waters C.L., Menk F.W., Bailey G.J., Fraser B.J., 1999. A Technique to Investigate Plasma Mass Density in the Topside Ionosphere using ULF Waves, J. Geophys. Res., 104, 12723.

Radoski, H.R., 1970. The resonance barrier theory of hydromagnetic waves, J. Geomagn. Geoelec., 22, 361.

Radoski, H.R., 1967. Highly asymmetric MHD resonances, J. Geophys. Res., 72, 4026.

Rankin, R., Lu, J. Y., Marchand, R., Donovan, E. F., 2004. Spatiotemporal characteristics of ultra-low frequency dispersive scale shear Alfven waves in the Earth's magnetosphere, Phys. Plasmas 11, 1268.

Samson, J.C., Wallis D.D., Hughes T.J., Creutzberg F., Ruohoniemi J.M., Greenwald, R.A., 1992. Substorm Intensifications and Field Line Resonances in the Nightside Magnetosphere, J. Geophys. Res., 97, 8495.

Sen, A.K., 1965. The Stability of the Magnetospheric Boundary, Planet. Space Sci., 13, 131.

Sibeck, D.G., 1994. Transient and quasi-periodic (5-15 min) events in the outer magnetosphere, in *Solar Wind Sources of Magnetospheric ULF Waves, Geophys. Monogr. Ser.* vol. 81, edited by M.J. Engebretson, K. Takahashi, and M. Scholer, p. 173, AGU, Washington, D.C.

Singer, H.J., Southwood, D.J., Walker, R.J., Kivelson, M.J., 1981. Alfven Wave Resonances in a Realistic Magnetospheric Magnetic Field Geometry, J. Geophys. Res., 86, 4589.

Southwood, D.J., 1968. The hydromagnetic stability of the magnetospheric boundary, Planet. Space Sci., 16, 857.

Southwood, D.J., 1974. Some features of field line resonances in the magnetosphere, Planet. Space Sci., 22, 483.

Tamao, T., 1966. Transmission and Coupling Resonance of Hydromagnetic Disturbances on the Non-Uniform Earth's Magnetosphere, Sci. Rep. Tohoku Univ., Ser. 5, 17, 43.

Tsyganenko, N.A., 1989. A Magnetospheric Magnetic Field Model with a Warped Tail Current Sheet, Planet. Space Sci., 37, 5.

Tsyganenko, N.A., Stern, D.P., 1996. Modeling the global magnetic field of the large-scale Birkeland current systems, J. Geophys. Res., 101, 27187.

Tsyganenko, N. A., 2002. A model of the near magnetosphere with a dawn-dusk asymmetry 2: Parameterisation and fitting to observations, J. Geophys. Res., 107, doi:

10.1029/2001JA000220.

Troitskaya, V.A., Gul'elmi A.V., 1967. Geomagnetic micropulsations and diagnostics of the magnetosphere, Space Sci. Rev., 7, 689.

Waters, C.L., Menk, F.W., Fraser, B.J., 1991. The resonance structure of low latitude Pc3 geomagnetic pulsations, Geophys. Res. Lett., 18, 2293.

Waters, C.L., Samson J.C., Donovan E.F., 1995. The temporal variation of the frequency of high latitude field line resonances, J. Geophys. Res., 100, 7987.

Waters, C.L., Samson J.C., Donovan E.F., 1996. Variation of plasmatrough density derived from magnetospheric field line resonances, J. Geophys. Res., 101, 24737.

Wright, A.N., 1992. Coupling of fast and Alfven modes in realistic magnetospheric geometries, J. Geophys. Res., 97, 6429.

Wright, A.N., Evans, N.W., 1991. Magnetic geometries that carry decoupled transverse or compressional magnetic field oscillations, J. Geophys. Res., 96, 209.

**Figures**

Figure 1. Cross phase spectra showing the change in ULF field line resonant frequencies with time and latitude from the CANOPUS magnetometer data for 9 February, 1995.

Figure 2. Plasma mass densities obtained from the FLRs shown in Fig. 1 and using the T01_01 magnetic field model.

Figure 3. Proton number densities obtained when using the dipole (solid), T89 (dotted), T96_01 (dashed), and T01_01 (dash-dot) magnetic field models.

Figure 4. (a) Changes in MLT where the magnetic field models trace to $Z_{GSM}$=0 compared with the MLT on the same field line at 120km altitude. (b) The location of $Z_{GSM}$=0 for the dipole (solid), T89 (dotted), T96_01 (dashed), and T01_01 (dash-dot) magnetic field models.

Figure 5. Proton number densities for the active day case for the dipole (solid), T89 (dotted), T96_01 (dashed), and T01_01 (dash-dot) magnetic field models.

Figure 6. Magnetic field properties for the active day case. (a) Changes in MLT where the magnetic field models trace to $Z_{GSM}$=0 compared with the MLT on the same field line at 120km altitude for the dipole (solid), T89 (dotted), T96_01 (dashed), and T01_01 (dash-dot) magnetic field models.. (b) Magnetic field model field line traces viewed above the XY plane.

Figure 7. Percentage difference in plasma mass densities when assuming the toroidal compared with the poloidal mode. (a) Quiet magnetic conditions (b) Active conditions.

Figure 8. Proton number densities when using the T01_01 magnetic field model and for $r^0$ (solid) and $r^6$ (dotted) plasma mass density functions assuming toroidal oscillations. The densities obtained assuming poloidal oscillation are also shown (dashed).

| Station pair | Geo. latitude | Geo. longitude | CGM latitude |
|---|---|---|---|
| RAN:ESK | 61.965 | 266.920 | 72.3 |
| ESK:FCH | 59.935 | 265.935 | 70.3 |
| FCH:BCK | 58.240 | 265.875 | 68.7 |
| BCK:GIL | 57.050 | 265.595 | 67.5 |
| GIL:ISL | 55.120 | 265.350 | 65.6 |
| ISL:PIN | 52.030 | 264.650 | 62.6 |

Table 1: Geographic coordinates and CGM latitudes corresponding to the midpoints of magnetometer pairs used in this study.

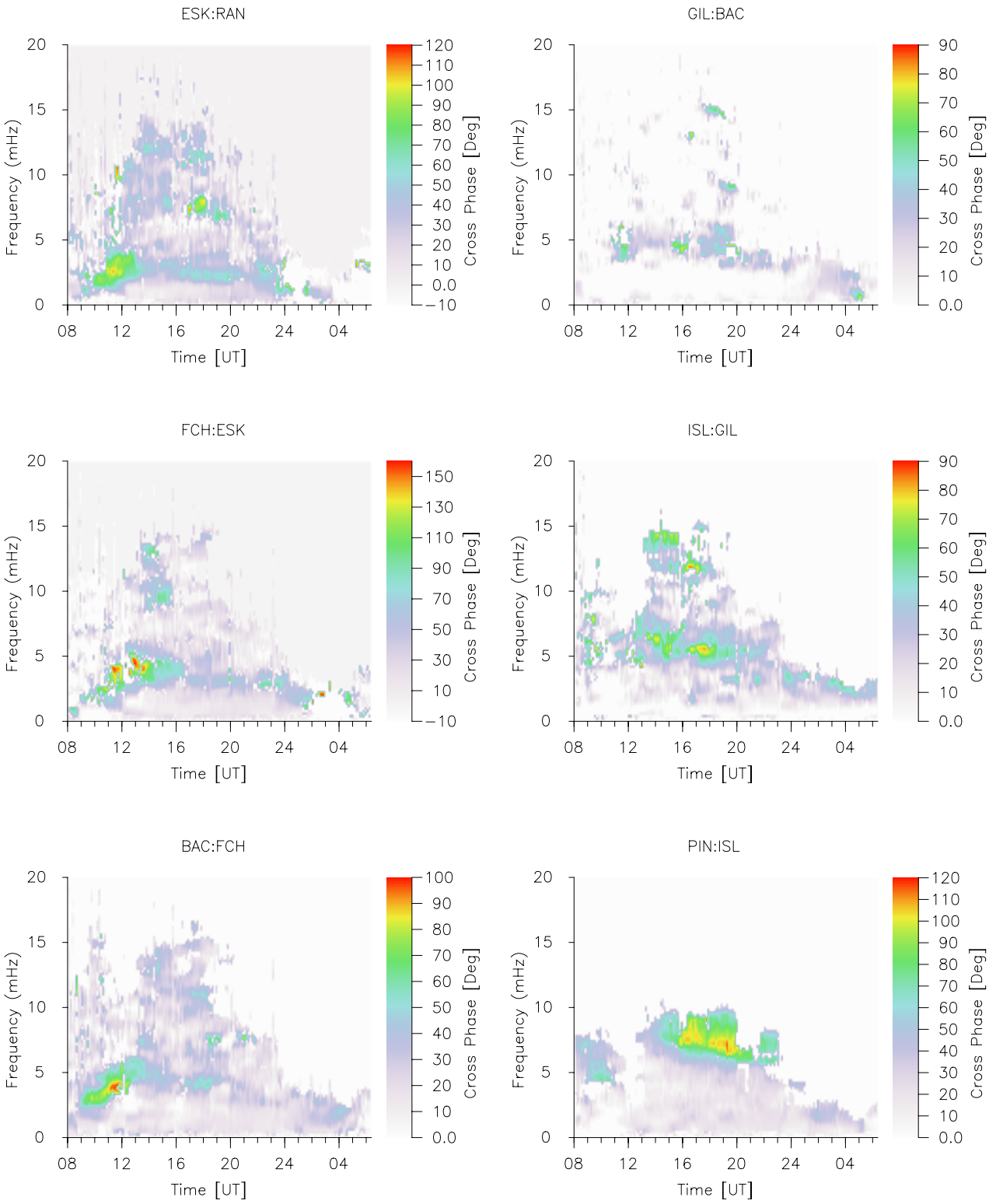


Fig 1. Cross phase spectra showing the change of FLRs with time and latitude from the CANOPUS magnetometer data for 9 Feb. 1995.

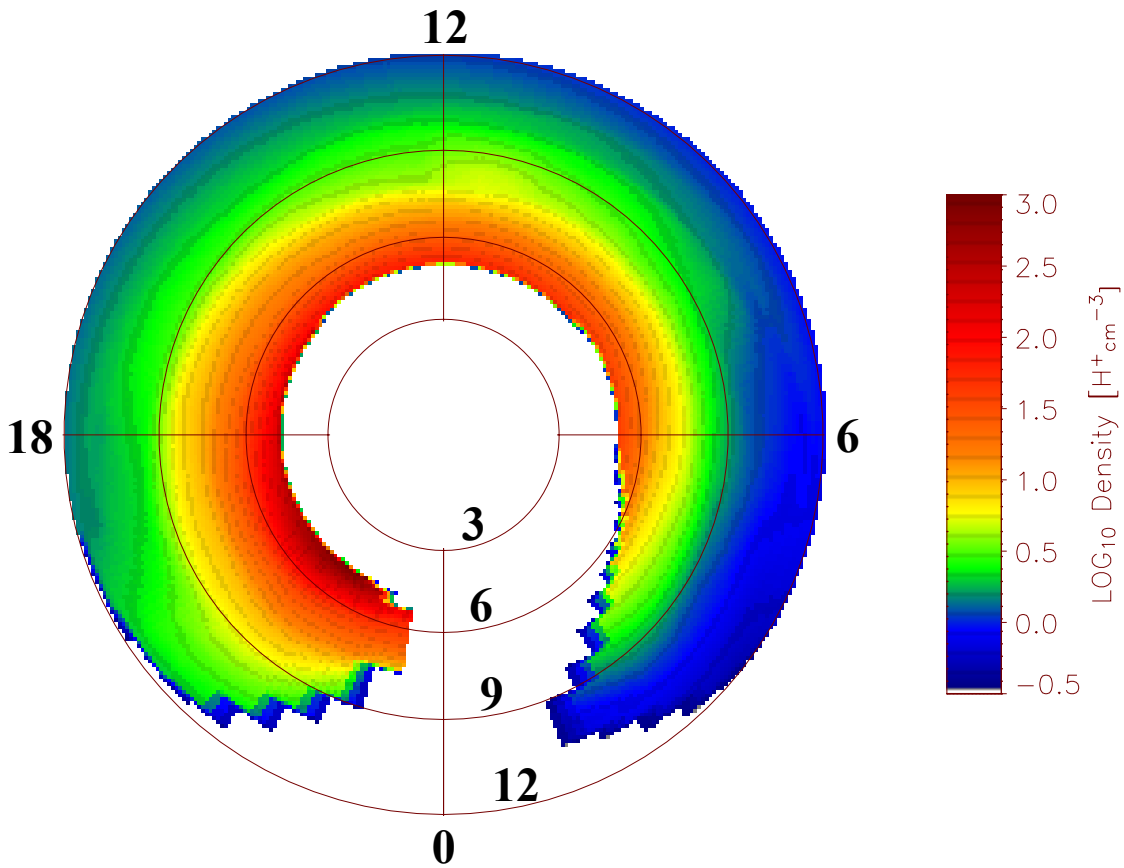


Fig 2. Plasma mass density from FLRs in Fig. 1 and using the T01_01 magnetic field model

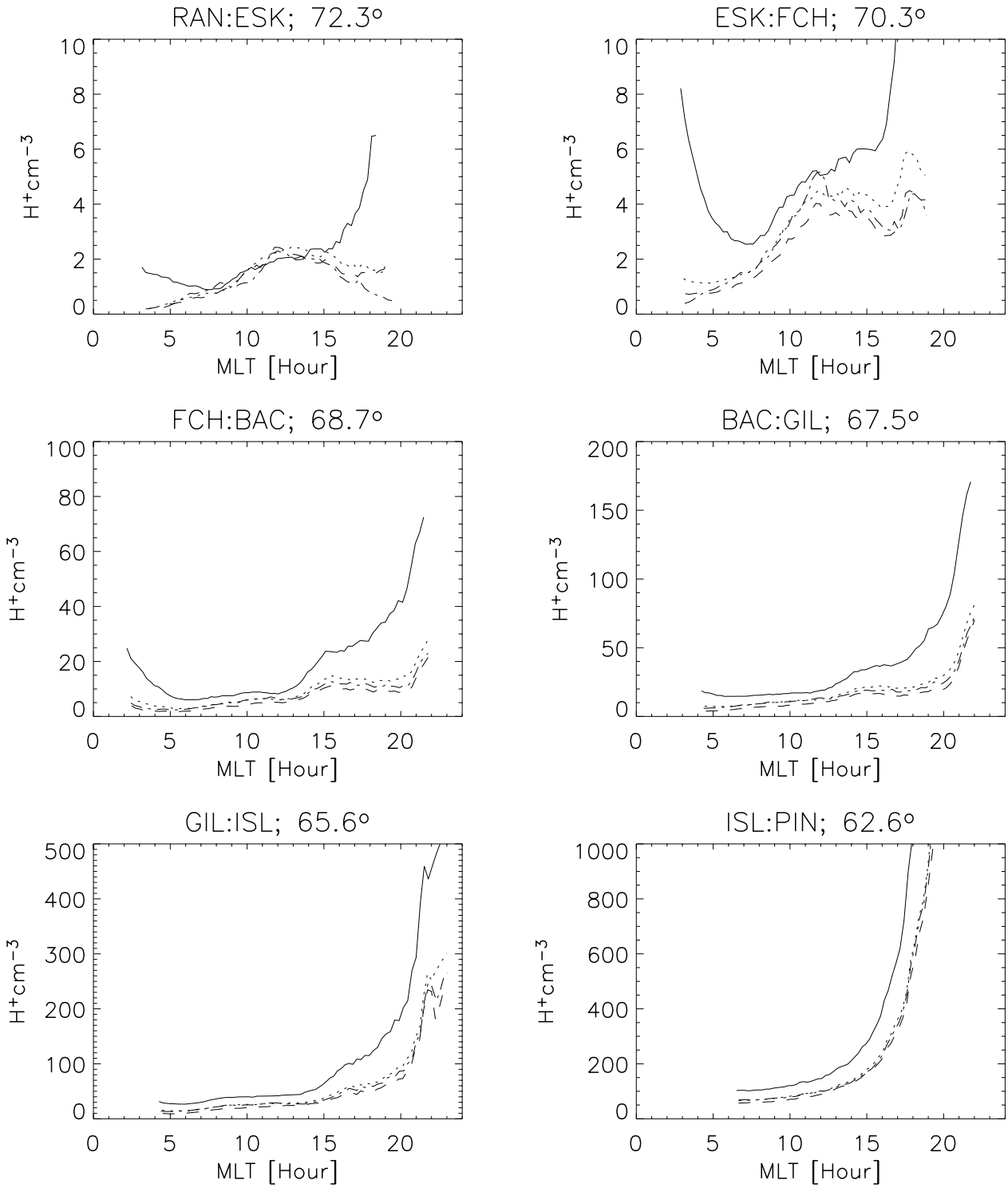


Fig 3. Proton number density for dipole (solid), T89 (dotted), T96 (dashed), T01 (dash-dot) magnetic field models.

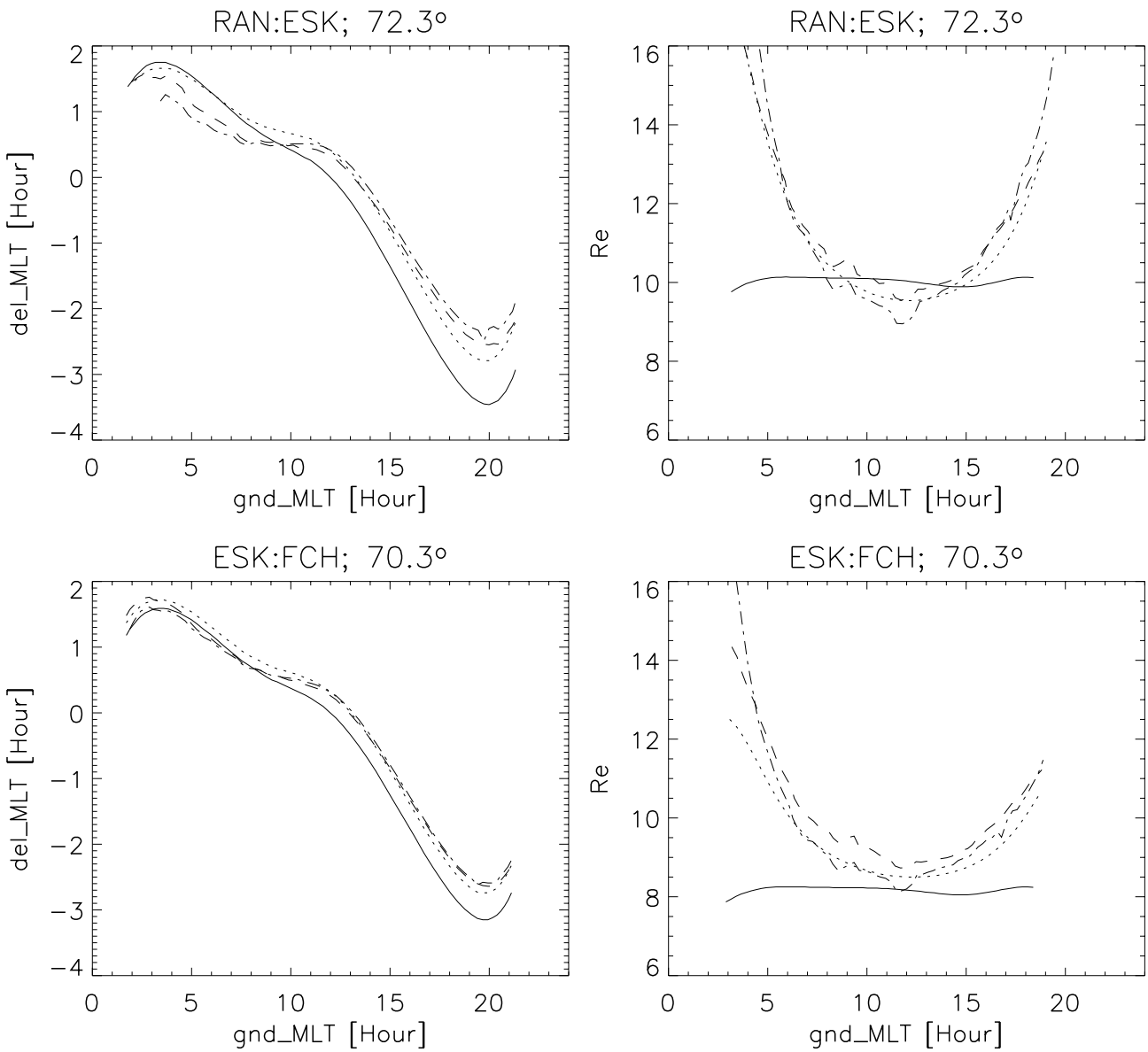


**(a)** **(b)**

Fig 4. (a) Field model MLT shift in Zgsm=0, (b) Field model Zgsm crossing point for the dipole (solid), T89 (dotted), T96 (dashed), T01 (dash-dot) magnetic field models.

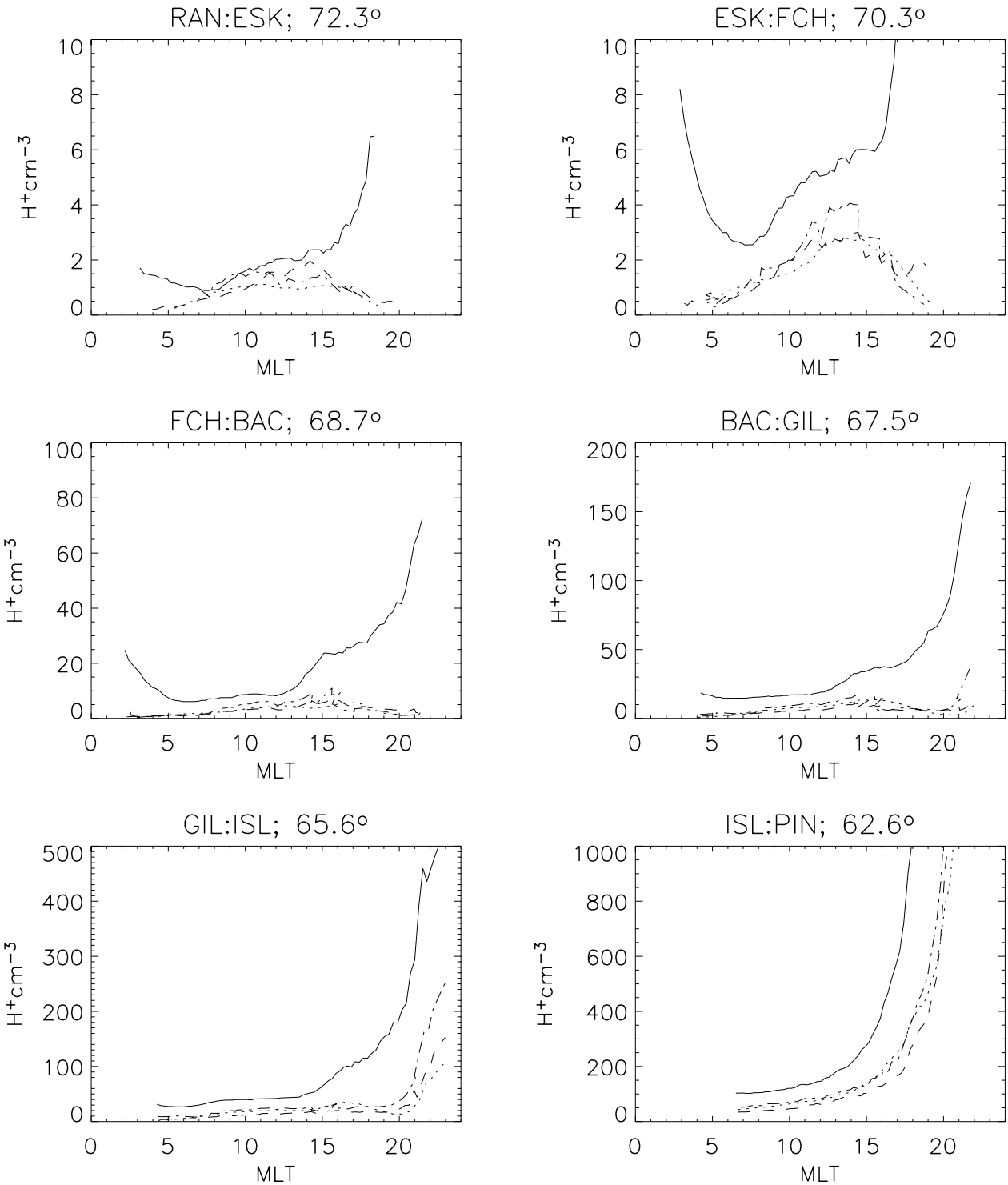


Fig 5. Proton number densities for active day for various field models; dipole (solid), T89 (dotted), T96 (dashed), T01 (dash-dot).

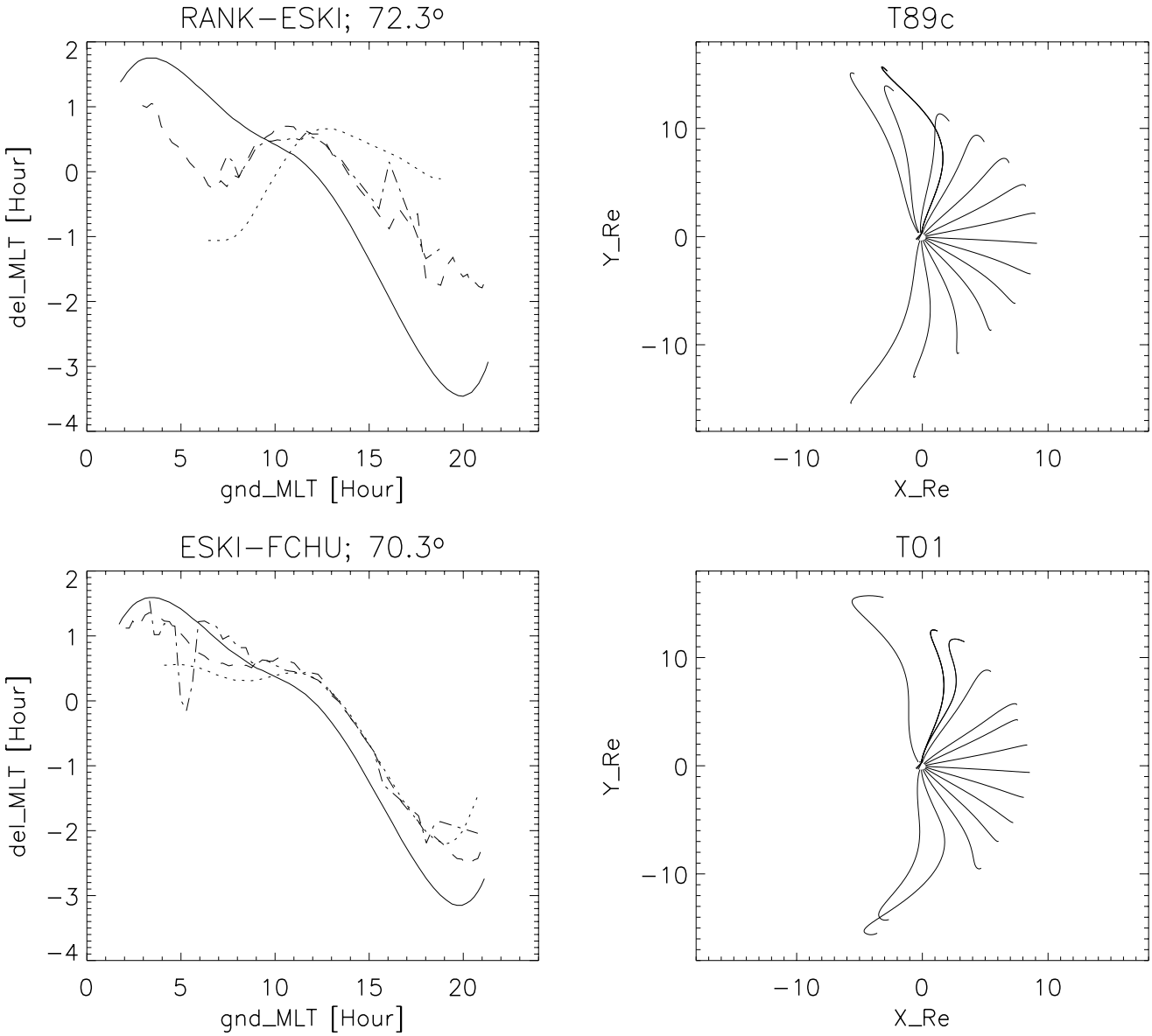


Fig 6. (a) Field model MLT shift in Zgsm=0,
(b) Field model XY projection

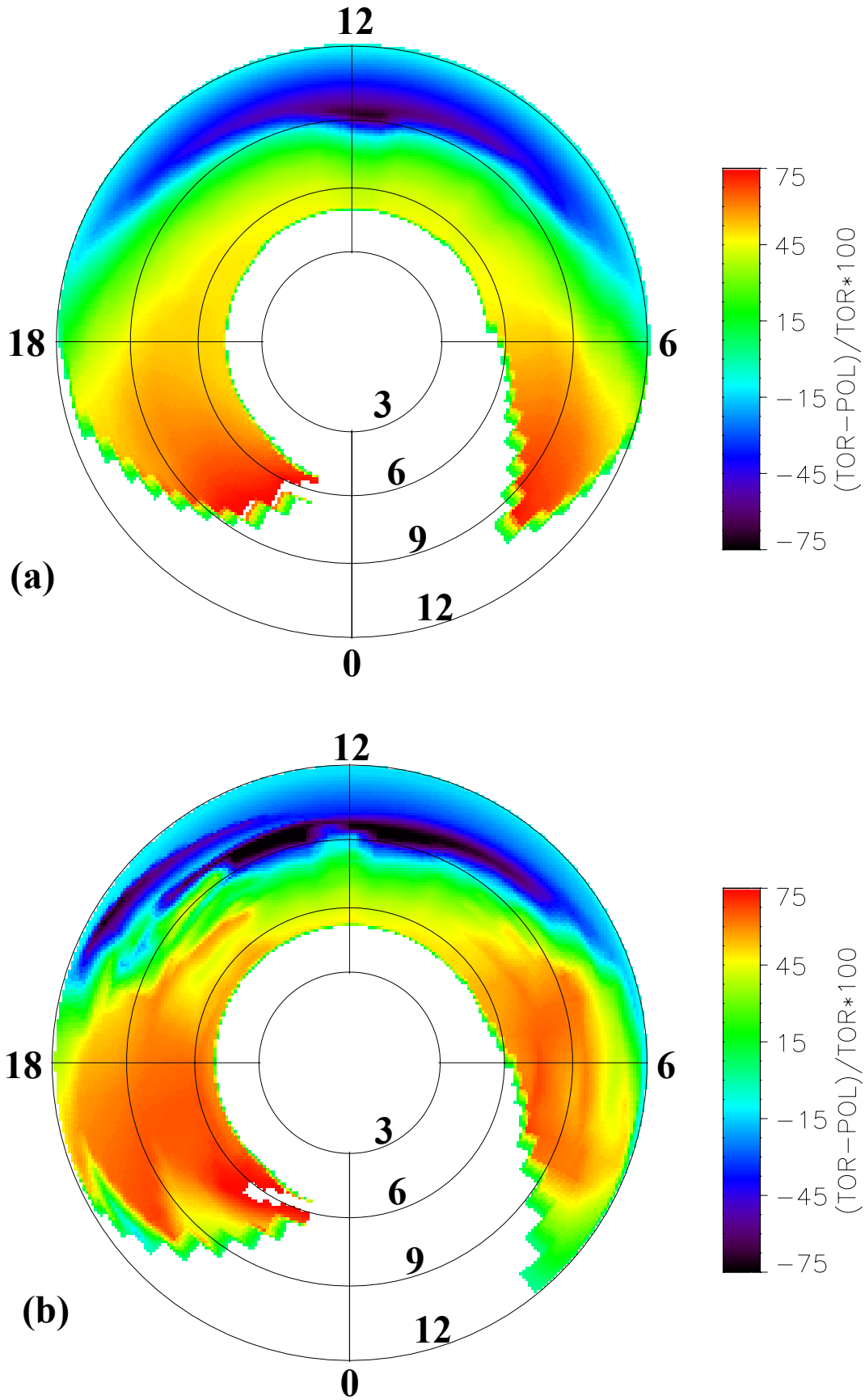


Fig 7. Percentage difference in mass densities when assuming the toroidal compared with the poloidal mode. (a) Quiet magnetic conditions (b) Active conditions

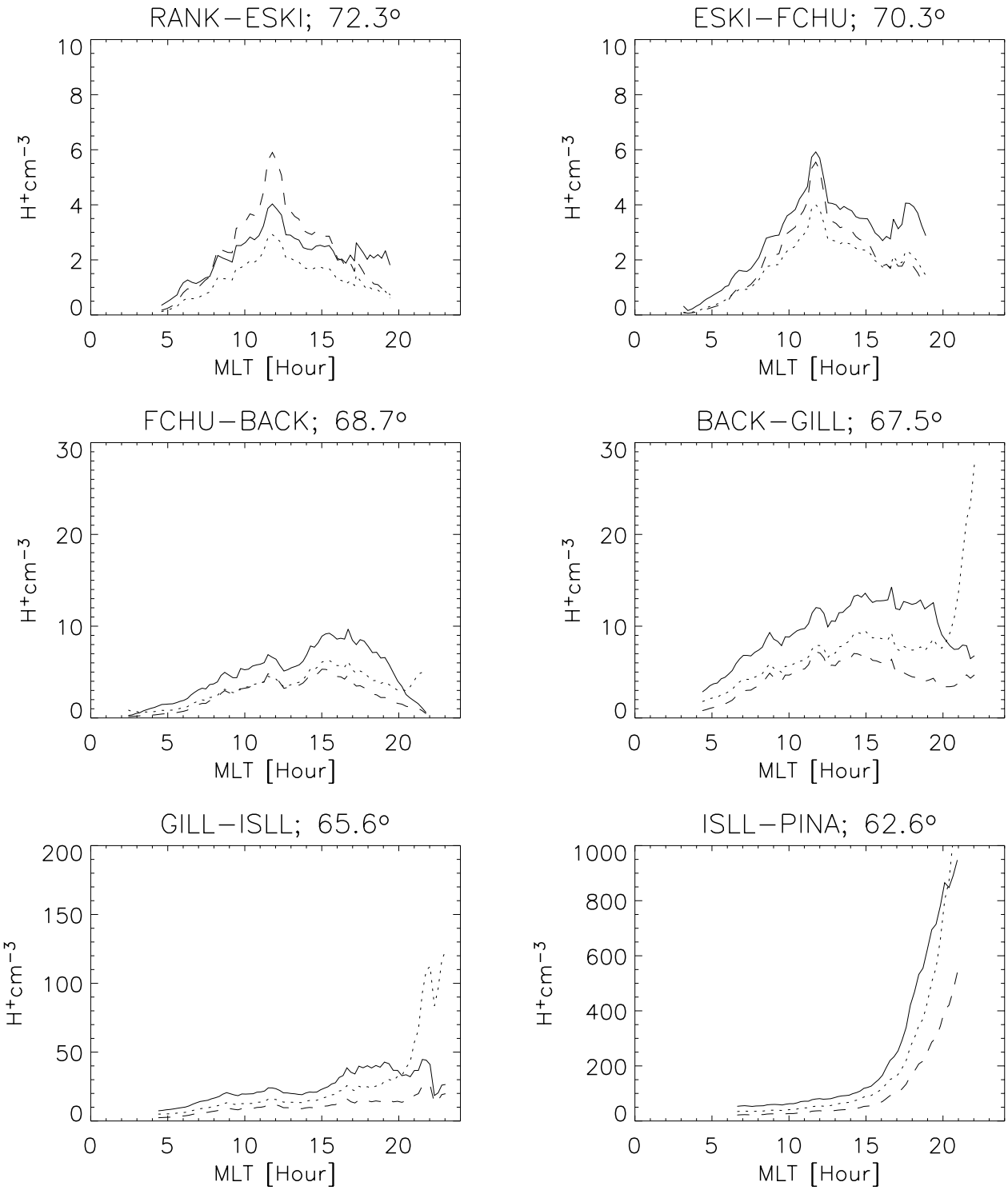


Fig 8. Proton number densities for T01 model and for $r^0$ (solid) and $r^6$ (dotted) plasma mass density functions assuming toroidal oscillations. The densities obtained assuming poloidal oscillation is also shown (dashed).